

Compensation Between Activation Entropy and Enthalpy in Reactions of Aromatic Hydrocarbons Catalyzed by Solid Acids

Koshiro Nakamura^a, Ryo Mizuta^a, Satoshi Suganuma^b, Etsushi Tsuji^a and Naonobu Katada^{a*}

^aDepartment of Chemistry and Biotechnology, Graduate School of Engineering, Tottori University, 4-101 Koyama-cho Minami, Tottori 680-8552, Japan

^bCenter for Research on Green Sustainable Chemistry, Faculty of Engineering, Tottori University, 4-101 Koyama-cho Minami, Tottori 680-8552, Japan

*Corresponding author: katada@chem.tottori-u.ac.jp Phone/fax +81-857-31-5684

Abstract

Reaction rates of toluene disproportionation (A) and cumene cracking (B) normalized by the number of Brønsted acid sites were analyzed on aluminosilicates. The activation entropy showed linear and compensatory relationship against the activation enthalpy. The slope of entropy-enthalpy plot was in the order of (B) > (A) > small alkane cracking, whereas the intercept on the horizontal axis was in the order of propane and isobutane cracking > linear C4-8 alkanes and iso-pentane cracking > (A) > (B). The former is consistent with the bulkiness of reactant, while the latter is consistent with intrinsic difficulty of formation of intermediate cations.

Keywords: Activation entropy, Activation enthalpy, Zeolite, Silica-alumina, Toluene disproportionation, Cumene cracking.

Introduction

Aluminosilicates including zeolites and amorphous silica-aluminas are important solid acid catalysts [1,2]. Alkane cracking is one of the representative use of the aluminosilicate solid acid catalysts [3-5], whereas various reactions like toluene disproportionation are operated for conversion

of mono-cyclic aromatic hydrocarbons [6-8]. Kinetic analysis is a classic method for investigation of these catalysis, but recent advances in analysis of physicochemical properties of solids may give new insights through the kinetic analysis.

We have developed a method of ammonia IRMS-TPD (infrared mass spectroscopy temperature-programmed desorption) to quantify the number and strength of Brønsted and Lewis acid sites [9], giving the reaction rate normalized by the number of Brønsted acid site. For small alkane cracking in the mono-molecular mechanism region, we have found a linear relationship between the activation enthalpies (hereafter $\Delta H^{*\circ}$ [J mol⁻¹]) and the enthalpies of ammonia desorption from Brønsted acid sites (ΔH_{NH_3} [J mol⁻¹]) on various aluminosilicates [10]. In addition, the activation entropy based on the number of Brønsted acid site ($\Delta S^{*\circ}$ [J K⁻¹ mol⁻¹]) showed a linear and compensatory relationship against $\Delta H^{*\circ}$ in which the larger the enthalpy, the larger the entropy [11].

The compensation effect gives information about the structure of intermediate on the rate determining step. The effect indicates that an active site with lower activation enthalpy holds the intermediate more tightly, losing the freedom of movement of the intermediate and resulting in the low entropy. Thermodynamic analyses in the host-guest complexes with various molecular structures clarified that the slope of the plots of ΔS against ΔH (entropy and enthalpy changes, respectively, of the association of host and guest molecules) shows the extent of complexity of host-guest complex, whereas the intercept on the vertical axis (ΔS at $\Delta H = 0$) shows difference in the freedom between the reactant in solution and the hosted complex [12].

The compensatory relationship between $\Delta S^{*\circ}$ and $\Delta H^{*\circ}$ or pre-exponential factor and activation energy [13] was found in various adsorption [14], non-catalytic and catalytic reactions [15-20]. In the early studies, various speculations and proposals were presented for the origin [17]. However, advances in the host-guest chemistry based on experiments with the molecular structures systematically varied has clearly evidenced that the compensation effect was due to the tendency in which the tightly bounded complex lost the freedom of movement as above [12].

Subsequently to the small alkane cracking [11], in the present study, we measured the kinetic

parameters in two reactions of mono-cyclic aromatic hydrocarbons, i.e, cracking (dealkylation) of cumene (2-phenylpropane) and disproportionation of toluene. The former has been a typical test reaction of solid Brønsted acid catalyst [21,22], whereas the latter has been applied to the production of para-xylene [23,24]. The relationships between $\Delta S^{*\circ}$ and $\Delta H^{*\circ}$ are related with nature of these important reactions.

(One paragraph removed)

Experimental

Table 1 shows the employed catalysts with their acidic properties. Samples of ZSM-5 zeolite (zeolites with MFI framework structure) were prepared by ion exchange of Na-ZSM-5 samples commercially available. A sample of Y zeolite (zeolite with FAU structure) was also prepared by ion exchange from Na-Y, and N-USY (ultrastable Y) was prepared by steaming of the above Y zeolite sample followed by NH_4NO_3 treatment [25]. In addition, some samples of mordenite (zeolite with MOR structure), zeolite β (zeolite with *BEA structure) and amorphous silica-alumina were employed as received.

The IRMS-TPD method was applied to measure the desorption profile of ammonia from each of Brønsted and Lewis acid sites as already described [9]. The enthalpy of ammonia desorption, ΔH_{NH_3} was calculated by a curve-fitting method [26] using a theoretical equation [27].

Toluene disproportionation and cumene cracking were carried out, and the activation entropy $\Delta S^{*\circ}$ and enthalpy $\Delta H^{*\circ}$ were calculated using Eyring equation [28] as shown in Supporting Information.

Results and Discussion

As shown in our paper [29], rate of such a reaction as toluene disproportionation in the continuous flow method is influenced by the deactivation of catalyst, even after it is weakened by co-feeding of hydrogen. The conversion at time on stream = 0 was estimated as shown in Supporting

Information, and kinetic analysis was carried out based on it.

Then, linear relationships were observed between $\ln \frac{k}{T}$ against $\frac{1}{T}$ in all the cases (Figure S3). Values of $\Delta H^{*\circ}$ and $\Delta S^{*\circ}$ are calculated from the slopes and intercepts.

Figure 1 shows the plots of $\Delta H^{*\circ}$ in various reactions against ΔH_{NH_3} from Brønsted acid site (shown in Table 1) as an index of Brønsted acid strength. In the case of alkane cracking, $\Delta H^{*\circ}$ was approximately dependent on the Brønsted acid strength; the higher the ammonia desorption enthalpy ΔH_{NH_3} , the lower the activation enthalpy $\Delta H^{*\circ}$. A few exceptional cases (MFI and in some cases of MOR) showed exceptional behaviors, suggesting that very small micropores may disturb the $\Delta H^{*\circ}$ - ΔH_{NH_3} relationship, but in most cases, simple relationships were observed as the stronger the Brønsted acid sites, the higher the activity [11]. However, $\Delta H^{*\circ}$ in the toluene disproportionation and cumene cracking were not related with ΔH_{NH_3} . It is naturally speculated that the reactions of aromatic molecules were more strongly influenced by the steric effects due to the pores of catalysts, especially in the cases of microporous zeolites, disturbing the influence of Brønsted acid strength.

Figure 2 shows the plots of $\Delta S^{*\circ}$ against $\Delta H^{*\circ}$ in the tested reactions. The linear relationships between them were found in all the reactions. This implies that the reaction rate was given by some simple principles throughout these reactions.

The slopes in these plots were [cumene cracking] > [toluene disproportionation] > [C3-8 alkane cracking], as shown in Table 3. Inoue et al. found that the slope of plots of ΔS against ΔH in host-guest chemistry showed the degree of complexity of host-guest complex [12]. Accordingly, the slope in the present study should show the complexity of transition state on the rate determining step. The complexity of speculated transition states (Table 3) is hence estimated as $\mathbf{4} > \mathbf{3} > \mathbf{1} \approx \mathbf{2}$. The order ($\mathbf{4}, \mathbf{3}$) > $\mathbf{1} \approx \mathbf{2}$ is naturally understood from the molecular structures, but the order $\mathbf{4} > \mathbf{3}$ needs discussion. It can be explained as that the rotation around the cation part ($-\text{CH}^+$) of $\mathbf{3}$ is possible, because the center carbon has only one hydrogen atom. On the contrary, the cation part in $\mathbf{4}$ [$-\text{C}^+(\text{CH}_3)_2$] is fixed by two methyl groups, as reflected by the slope.

In addition, the slopes of $\Delta S^{*\circ}$ - $\Delta H^{*\circ}$ plots in the present catalytic reactions (0.87 to 2.0 K⁻¹)

were generally similar or larger than those of ΔS - ΔH plots in the host-guest association (0.51 to 1.07 K⁻¹ in [12] and 0.51 to 1.03 K⁻¹ in [30]). It is reasonable that a transition state trapped by the solid surface has low freedom of movement compared to a molecule in a solution.

The intercept on the vertical axis of ΔS - ΔH plot has been proposed by Inoue et al. to show the extent of entropy gain by desolvation in the host-guest association [12]; $T\Delta S_0$, where T was 298 K, and ΔS_0 was the intercept on the vertical axis of ΔS - ΔH plot, was 0.0 to 5.0 kcal mol⁻¹ [12] and 9.6 to 22.5 kJ mol⁻¹ in [30], equivalent to 0 to 70 and 32 to 76 J K⁻¹ mol⁻¹ of ΔS_0 , respectively. The positive values indicate the gain of freedom due to separation from the solvent molecules. On the contrary, the intercept on the vertical axis of $\Delta S^{*\circ}$ - $\Delta H^{*\circ}$ plot in this study was -282 to -226 J K⁻¹ mol⁻¹ (Table 3), large negative values, showing loss of freedom of gas molecules by trapping with the solid surface.

We here propose that the intercept on the horizontal axis of $\Delta S^{*\circ}$ - $\Delta H^{*\circ}$ plot shows the intrinsic activation barrier, reflecting the chemical nature of the reaction but not influenced by the freedom of movement, because it is $\Delta H^{*\circ}$ at $\Delta S^{*\circ} = 0$ or $\Delta G^{*\circ}$ (activation Gibbs energy defined by $\Delta G^{*\circ} = \Delta H^{*\circ} - T\Delta S^{*\circ}$) at $T = 0$. This parameter was 130 to 270 kJ mol⁻¹ in the present catalytic reactions (Table 3), reflecting that the activation process is endothermic. On the contrary, the intercept on the horizontal axis of ΔS - ΔH or $T\Delta S$ - ΔH plot in the host-guest association was -33 to 0 kJ mol⁻¹ in literature [12,30] [calculated using above values by (intercept on horizontal axis) = - (intercept on vertical axis) / (slope)], in agreement with that the reported host-guest association was in most cases spontaneous reaction and hence exothermic.

In addition, the intercept on the horizontal axis of $\Delta S^{*\circ}$ - $\Delta H^{*\circ}$ plot was [propane and isobutane cracking] > [linear C4-8 alkanes and isopentane cracking] > [toluene disproportionation] > [cumene cracking], as shown in Table 3. From the molecular structures, the difficulty of formation is speculated to be **1** [non-classical carbonium (alkanium) cation associating a primary carbon atom] > **2** (carbonium associating only secondary and/or tertiary carbon atoms) > **3** [carbenium (alkenium) cation at the secondary part] > **4** (carbenium at the tertiary part). This is in good agreement with the

observed values.

We still have speculations in the above discussion, and further investigations should be necessary, but the present observations show a possibility of the traditional kinetic study to give a deep insight of the catalytic reactions, especially about what controls the reaction behavior.

Conclusions

Kinetic analysis based on the reaction rate normalized by the number of Brønsted acid sites on various aluminosilicate solid acid catalysts showed the compensatory relationship between the activation entropy $\Delta S^{*\circ}$ and activation enthalpy $\Delta H^{*\circ}$. The slope of plots of $\Delta S^{*\circ}$ against $\Delta H^{*\circ}$ was in the order of [cumene cracking] > [toluene disproportionation] > [C3-8 alkane cracking]. Bulky molecular size and shape of the reactant tended to result in the steep slope. The intercept on the horizontal axis was [C3 and C4 monomethyl branched alkane cracking] > [linear C4-8 and C5 monomethyl branched alkane cracking] > [toluene disproportionation] > [cumene cracking], in agreement with the estimated difficulty of formation of transition states.

Acknowledgement: This study was partly supported by JSPS (Japan Society for Promotion of Science) KAKENHI 16H04568 and 16K14093.

[1] A. Corma, Inorganic Solid Acids and Their Use in Acid-Catalyzed Hydrocarbon Reactions, *Chem. Rev.* 95 (1995) 559–614.

[2] A. Corma, A. Martinez, Zeolites and Zeotypes as Catalysts, *Adv. Mater.* 7 (1995) 137–144.

[3] V.J. Frilette, W.O. Haag, R.M. Lago, Catalysis by crystalline aluminosilicates: Characterization of intermediate pore-size zeolites by the “Constraint Index”, *J. Catal.* 67 (1982) 218–222.

[4] H. Krannila, W. O. Haag, B. C. Gates, Monomolecular and Bimolecular Mechanisms of Paraffin Cracking: n-Butane Cracking Catalyzed by HZSM-5, *J. Catal.* 135 (1992) 115-124.

[5] I.E. Maxwell, W.H.J. Stork WHJ, Hydrocarbon Processing with Zeolites, *Stud. Surf. Sci. Catal.* 137 (2001) 747–819.

-
- [6] S. Al-Khattaf, S.A. Ali, A.M. Aitani, N. Žilková, D. Kubička, J. Čejka, Recent Advances in Reactions of Alkylbenzenes Over Novel Zeolites: The Effects of Zeolite Structure and Morphology, *Catal. Rev. Sci. Eng.* 56 (2014) 333–402.
- [7] C. Perego, P. Ingallina, Combining Alkylation and Transalkylation for Alkylaromatic Production, *Green Chem.* 6 (2004) 274-279.
- [8] J. Čejka, B. Wichterlová, Acid-catalyzed Synthesis of Mono- and Dialkyl Benzenes over Zeolites: Active Sites, Zeolite Topology, and Reaction Mechanisms, *Catal. Rev.* 44 (2002) 375-421.
- [9] M. Niwa, K. Suzuki, N. Katada, T. Kanougi, T. Atoguchi, Ammonia IRMS-TPD Study on the Distribution of Acid Sites in Mordenite, *J. Phys. Chem. B* 109 (2005) 18749–18757.
- [10] N. Katada, K. Suzuki, T. Noda, W. Miyatani, F. Taniguchi, M. Niwa, Correlation of the Cracking Activity with Solid Acidity and Adsorption Property on Zeolites, *Appl. Catal. A: Gen.* 373 (2010) 208–213.
- [11] N. Katada, S. Sota, N. Morishita, K. Okumura, M. Niwa, Relationship between Activation Energy and Pre-exponential Factor Normalized by Number of Brønsted Acid Sites in Cracking of Short Chain Alkanes on Zeolites, *Catal. Sci. Technol.* 5 (2015) 1864–1869.
- [12] Y. Inoue, Y. Liu, L.-H. Tong, B.-J. Shen, D-S. Jin, Calorimetric Titration of Inclusion Complexation with Modified β -Cyclodextrins. Enthalpy-entropy Compensation in Host-guest Complexation: from Ionophore to Cyclodextrin and Cyclophane, *J. Am. Chem. Soc.* 115 (1993) 10637–10644.
- [13] G. Lente, *Deterministic Kinetics in Chemistry and Systems Biology*, Springer, Hyderabad, 2015.
- [14] D.H. Everett, The Thermodynamics of Adsorption. Part II.—Thermodynamics of Monolayers on Solids, *Trans. Faraday. Soc.* 46 (1950) 942–957.
- [15] A. Bhan, R. Gounder, J. Macht, E. Iglesia, Entropy Considerations in Monomolecular Cracking of Alkanes on Acidic Zeolites, *J. Catal.* 253 (2008) 221–224.
- [16] J.E. Leffler, JE The Enthalpy-Entropy Relationship and Its Implications for Organic Chemistry, *J. Org. Chem.* 20 (1955) 1202–1231.

-
- [17] A.K. Galwey, Compensation Effect in Heterogeneous Catalysis, *Adv. Catal.* 26 (1977) 247–322.
- [18] T.-K. Cheung, F.C. Jentoft, J.L. d'Itri, B.C. Gates, Protolytic Cracking of Low-molecular-weight Alkanes in the Presence of Iron- and Manganese-promoted Sulfated Zirconia: Evidence of a Compensation Effect, *Chem. Eng. Sci.* 52 (1997) 4607–4613.
- [19] L.E. Sandoval-Díaz, J.M. Martínez-Gil, C.A. Trujillo, The Combined Effect of Sodium and Vanadium Contamination upon the Catalytic Performance of USY Zeolite in the Cracking of n-Butane: Evidence of Path-dependent Behavior in Constable–Cremer Plots, *J. Catal.* 294 (2012) 89–98.
- [20] D.C. Longstaff, Development of a Comprehensive Naphtha Catalytic Cracking Kinetic Model, *Energy & Fuels* 26 (2012) 801–809.
- [21] A. Corma, B.W. Wojciechowski, The Catalytic Cracking of Cumene, *Catal. Rev. Sci. Eng.* 24 (1982) 1–65.
- [22] A.M. Youssef, A.I. Ahmed, S.E. Samra, Surface and Acidic Properties of Some Mixed Oxide Catalysts in Relation to Their Catalytic Activities, *Mater. Lett.* 10 (1990) 175–180.
- [23] J.S. Beck, D.H. Olson, S.B. McCullen, Selective Toluene Disproportionation Process (STDP) with ex-situ Selectivated Zeolite Catalyst, U. S. Patent 5367099, 1994.
- [24] T.-C. Tsai, S.-B. Liu, I. Wang, Disproportionation and Transalkylation of Alkylbenzenes over Zeolite Catalysts, *Appl. Catal., A: Gen.* 181 (1999) 355–398.
- [25] K. Okumura, T. Tomiyama, N. Morishita, T. Sanada, K. Kamiguchi, N. Katada, M. Niwa, Evolution of Strong Acidity and High-alkane-cracking Activity in Ammonium-treated USY Zeolites, *Appl. Catal., A: Gen.* 405 (2011) 8–17.
- [26] N. Katada, H. Igi, J.-H. Kim, Miki Niwa, Determination of the Acidic Properties of Zeolite by Theoretical Analysis of Temperature-Programmed Desorption of Ammonia Based on Adsorption Equilibrium, *J. Phys. Chem. B* 101 (1997) 5969–5977.
- [27] M. Niwa, N. Katada, M. Sawa, Y. Murakami, Temperature-Programmed Desorption of Ammonia with Readsorption Based on the Derived Theoretical Equation, *J. Phys. Chem.* 99 (1995)

8812-8816.

[28] S. Glasstone, K.J. Laidler, H. Eyring, *Theory of Rate Processes* McGraw-Hill, New York, 1941.

[29] D. Mitsuyoshi, K. Kuroiwa, Y. Kataoka, T. Nakagawa, M. Kosaka, K. Nakamura, S. Suganuma, Y. Araki, N. Katada, Shape Selectivity in Toluene Disproportionation into para-Xylene Generated by Chemical Vapor Deposition of Tetramethoxysilane on MFI Zeolite Catalyst, *Micropor. Mesopor. Mater.* 242 (2017) 118–126.

[30] Y. Lin, H. Wang, L.-H. Wang, H.-Y. Zhang, Complexation Thermodynamics of Water-soluble Calix[4]arene Derivatives with Lanthanoid(III) Nitrates in Acidic Aqueous Solution, *Thermochim. Acta* 414 (2014) 65-70.

Table 1 Employed aluminosilicate catalysts and their acidic properties

Catalyst	Origin	Structure	Si/Al	Number of acid sites / mol kg ⁻¹		Averaged enthalpy of ammonia desorption from Brønsted acid site (ΔH_{NH_3}) / kJ mol ⁻¹
				Brønsted	Lewis	
ZSM-5 (12) ^a	Na-ZSM-5 from Tosoh Corp. was ion-exchanged into NH ₄ -form.	MFI	12	1.15	0.00	139
ZSM-5 (15) ^a	Na-ZSM-5 from Mizusawa Chemical Industries Co. Ltd. was ion-exchanged into NH ₄ -form.	MFI	15	0.82	0.01	138
Y ^a	Na-Y from Tosoh Corp. was ion-exchanged into NH ₄ -form.	FAU	2.4	0.51	0.00	161
N-USY ^a	The above Y was steamed at 823 K and treated with 0.5 mol dm ⁻³ NH ₄ NO ₃ aq. [25]	FAU	2.3	0.52	0.13	134
mordenite ^b	JRC-Z-HM20 ^c	MOR	10	0.94	0.00	161
β (13) ^b	JRC-Z-HB25 (1) ^c	*BEA	13	0.46	0.06	138
β (75) ^b	JRC-Z-HB150 (1) ^c	*BEA	75	0.13	0.00	145
SAH-1 ^b	JRC-SAH-1 ^c	amorphous	2.1	0.32	0.17	113
SAL-2 ^b	JRC-SAL-2 ^c	amorphous	5.3	0.20	0.23	116
N631L ^b	Supplied from JGC Catalysts and Chemicals Ltd.	amorphous	5.7	0.26	0.02	111

a: ZSM-5 (12), ZSM-5 (15), Y and N-USY were stored as the NH₄-form, and converted into the H-form in the pre-treatment of ammonia IRMS-TPD measurements and catalytic tests.

b: Supplied as H-form and used as supplied.

c: Reference catalysts distributed by Catalysis Society of Japan.

Table 2 Kinetic parameters

Catalyst	Toluene disproportionation				Cumene cracking			
	E_a / kJ mol ⁻¹	A / s ⁻¹	ΔH^{*o} / kJ mol ⁻¹	ΔS^{*o} / J K ⁻¹ mol ⁻¹	E_a / kJ mol ⁻¹	A / s ⁻¹	ΔH^{*o} / kJ mol ⁻¹	ΔS^{*o} / J K ⁻¹ mol ⁻¹
ZSM-5 (12)	91	4.2×10^5	84	-154	85	5.1×10^6	81	-129
ZSM-5 (15)	181	3.4×10^{11}	172	-44	47	8.4×10^2	62	-167
Y	231	2.2×10^{15}	225	32	40	2.7×10^3	36	-197
N-USY	71	4.4×10^4	65	-174				
mordenite	206	8.0×10^{13}	200	5	38	39	33	-227
β (13)	94	2.0×10^6	88	-130	98	6.8×10^8	93	-79
β (75)	130	1.8×10^9	124	-94	36	1.8×10^3	36	-200
SAH-1	106	1.4×10^5	99	-163	79	2.3×10^6	74	-136
SAL-2	83	1.7×10^4	77	-180	74	1.4×10^6	70	-140
N631L	28	5.0	21	-248	45	1.3×10^3	41	-199

Table 3 Speculated key intermediates and parameters in plots of $\Delta S^{*\circ}$ against $\Delta H^{*\circ}$ of tested reactions

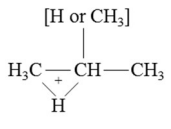
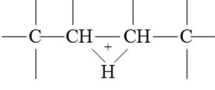
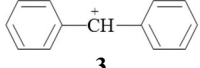
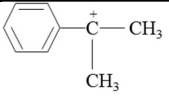
Reaction	Speculated key intermediate	Slope / K^{-1}	Intercept on vertical axis / $J K^{-1} mol^{-1}$	Intercept on horizontal axis / $kJ mol^{-1}$
Cracking of propane and isobutane	 <p style="text-align: center;">1</p>	0.901	-244	270
Cracking of C4-C8 linear alkanes and isopentane	 <p style="text-align: center;">2</p>	0.872	-226	255
Toluene disproportionation	 <p style="text-align: center;">3</p>	1.33	-245	184
Cumene cracking	 <p style="text-align: center;">4</p>	2.02	-282	136

Figure captions

Figure 1 Plots of $\Delta H^{*\circ}$ in cracking of (A) propane (black), butane (brown), iso-butane (2-methylpropane, red), pentane (grey), isopentane (2-methylbutane, green), hexane (blue) and octane (purple) [11], (B) toluene disproportionation (blue) and cumene cracking (red) against ΔH_{NH_3} from Brønsted acid site over MFI (◆), MOR (△), FAU (○) and *BEA (▽) zeolites, and amorphous silica alumina (□).

Figure 2 Plots of $\Delta S^{*\circ}$ against $\Delta H^{*\circ}$ in cracking of propane and iso-butane (green) [11], cracking of C4-C8 linear alkanes and isopentane (black) [11], toluene disproportionation (blue) and cumene cracking (red) over MFI (◇), MOR (△), FAU (○) and *BEA (▽) zeolites and amorphous silica alumina (□).

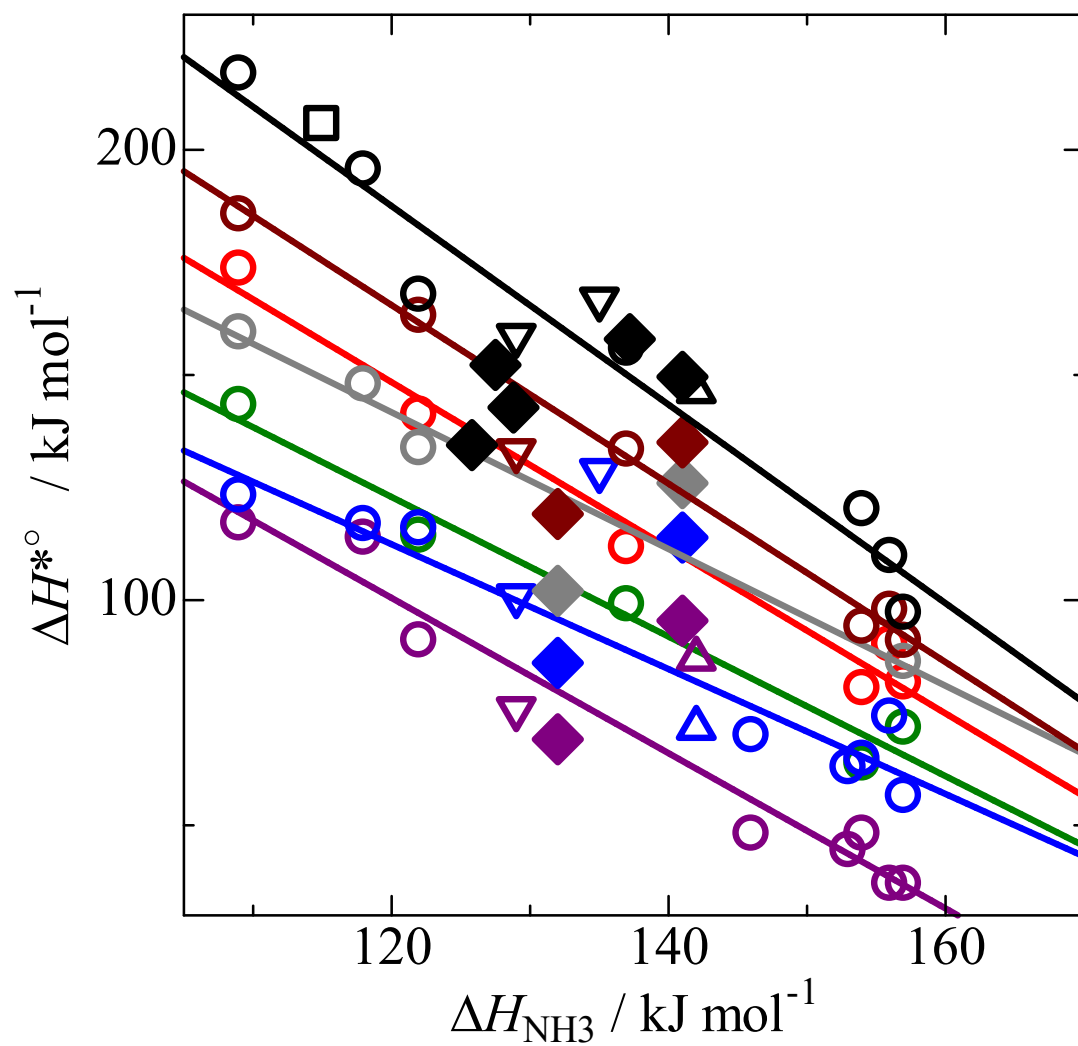


Figure 1 (A)

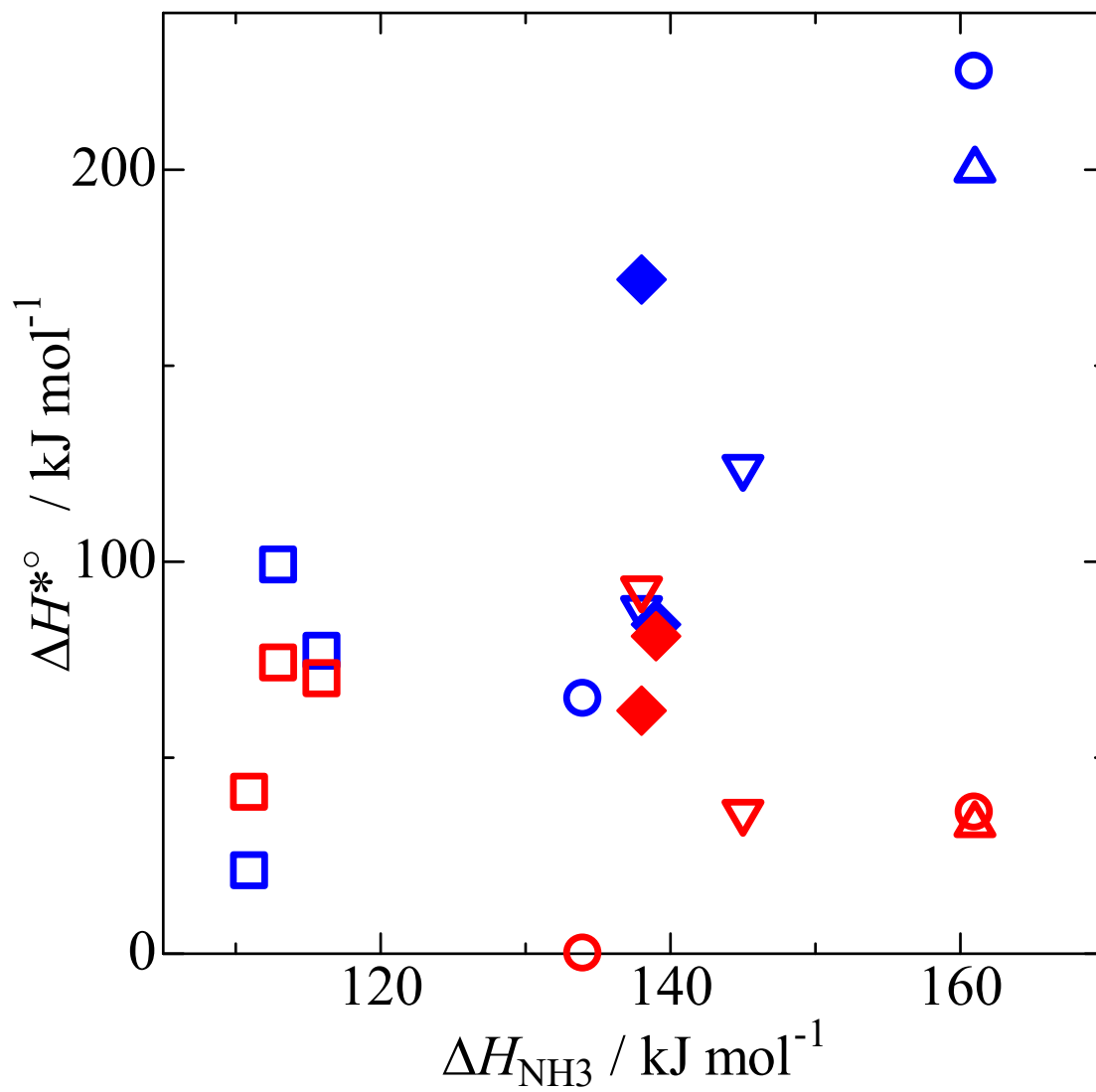


Figure 1 (B)

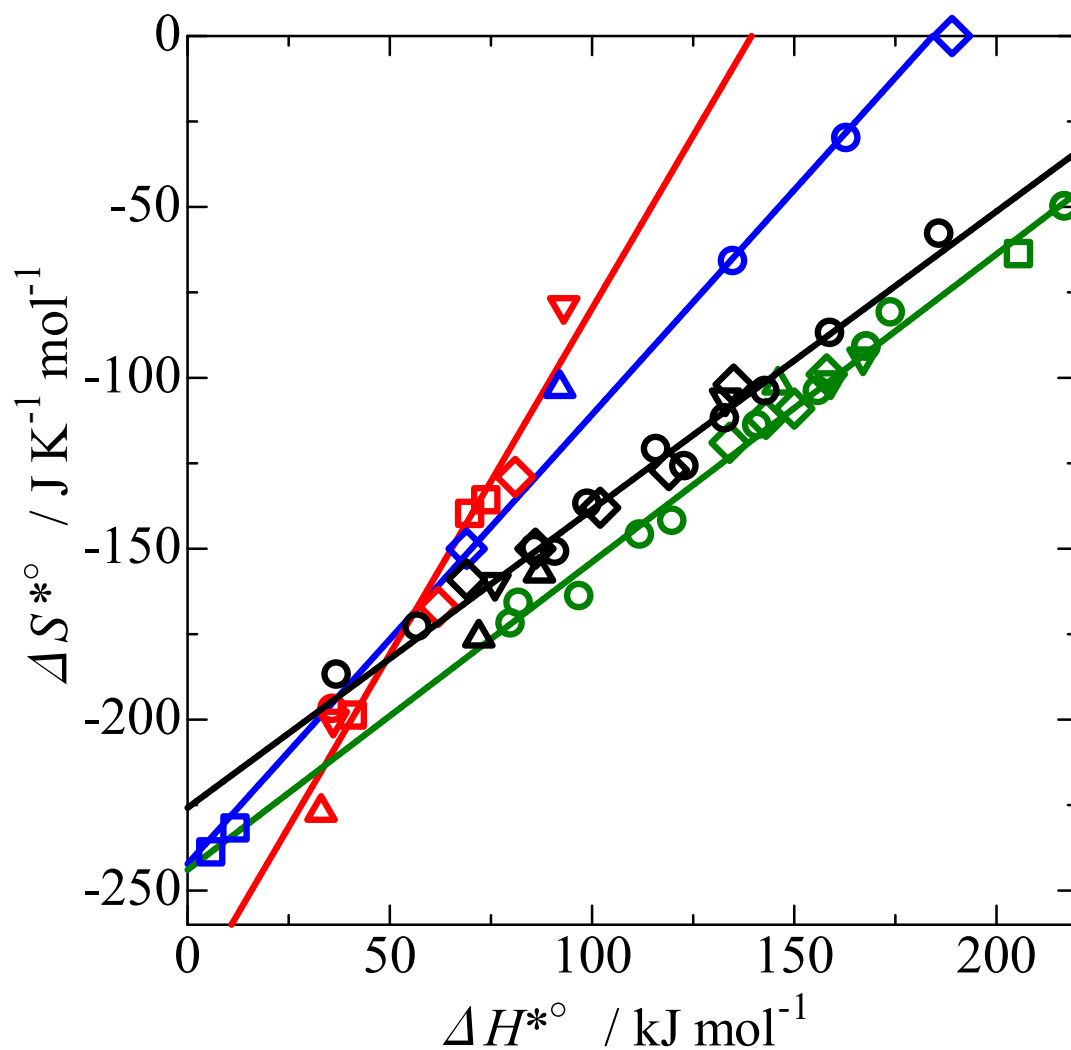


Figure 2